Supplementary Information

An insect-inspired, spike-based, in-sensor, and night-time collision detector based on atomically thin and light-sensitive memtransistors

Darsith Jayachandran[1], Andrew Pannone[1], Mayukh Das[1], Dipanjan Sen[1], Thomas F Schranghamer[1], and Saptarshi Das[1,2,3,4,]*

[1]Engineering Science and Mechanics, Penn State University, University Park, PA 16802, USA

[2]Electrical Engineering and Computer Science, Penn State University, University Park, PA 16802, USA

[3]Materials Science and Engineering, Penn State University, University Park, PA 16802, USA

[4]Materials Research Institute, Penn State University, University Park, PA 16802, USA

Supplementary Information 1.

A simple model was created that captures several major aspects of the response of an LGMD neuron to a looming stimulus. In an impending collision scenario, the projected size of the obstacle onto the photoreceptors within the locust's eye will increase over time as the distance between the two entities is reduced. This perceived increase in size of the obstacle will provoke an inhibitory and excitatory response in the two dendritic branches of the LGMD neuron. The combination of excitatory and inhibitory responses leads to a non-monotonic escape response that manifests as a peak in the spiking activity of the neuron that occurs well before the time of collision. The relationship between the firing rate of an LGMD neuron and the projected size of a looming stimulus can be expressed using Eq. S1 [1] shown below.

$$f(t) = \exp[logS' - \alpha S] = S' \exp[-\alpha S]\,;\ \alpha = tan^{-1}(\tfrac{2}{S_{TH}}) \qquad [S1]$$

Here, t represents time, while S and S_{TH} represent the perceived size of the looming object at time t and the perceived size threshold of the object, respectively. S_{TH} is an insect species dependent parameter that determines the perceived size threshold where the neural firing response reaches its climax [2]. To model the neural responses of the LGMD neuron, we assumed an object of size 50 mm approaching the insect from an initial distance of 900 mm at different approach velocities of 1.5 m/s, 0.6 m/s and 0.4 m/s. S_{TH} was taken empirically as 40 mm^2 for ease of calculation. Both the projected area (S) and the derivative of the projected area (S') were observed to increase with time. Even though S increases over time, the factor $exp(-\alpha S)$ exponentially decreases as described in Fig. 1c, designated as the inhibitory neural response of the model. The time rate of change of S' is the excitatory neural response of the model, given in Fig. 1d. Finally, the multiplicative neuronal output combining the inhibitory and excitatory modeled responses shows

a non-monotonic trend in neuronal spike frequency over time. A maximum spike frequency is reached prior to collision. The frequency values of the output were observed to be real fractions between 0 and 1. For simplicity of computation and discernable visual representation, we have multiplied the frequency with a factor of 10 and rounded off to the nearest integer values. As a result, adjacent points in time with similar spiking frequencies have been grouped together and represented with spikes corresponding to the relative magnitude of the firing frequency throughout the time interval. The firing frequency increases, reaches the maximum, and subsequently decreases in discrete steps, as evident from Fig. 1e. This variable discretization used in this bio-realistic model emulates the LGMD neuronal spiking responses found in biological studies.

Supplementary Information 2.

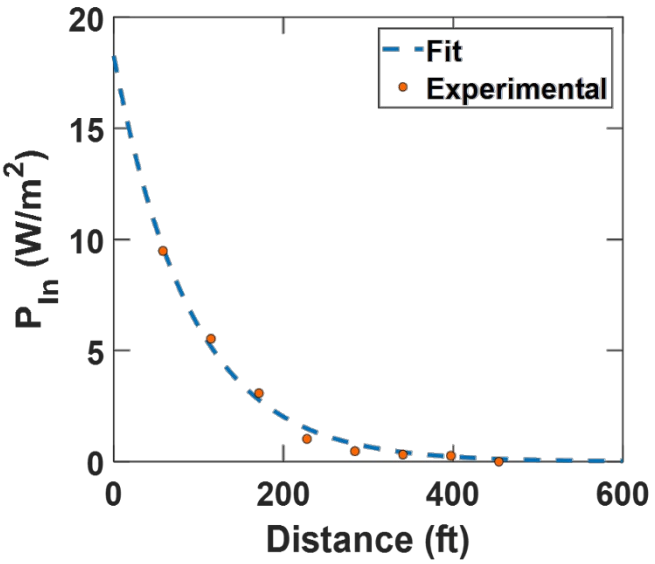

Figure S1. *P_{IN} plotted as a function of the distance (d_c) between the collision detector and the approaching car.*

Supplementary Information 3.

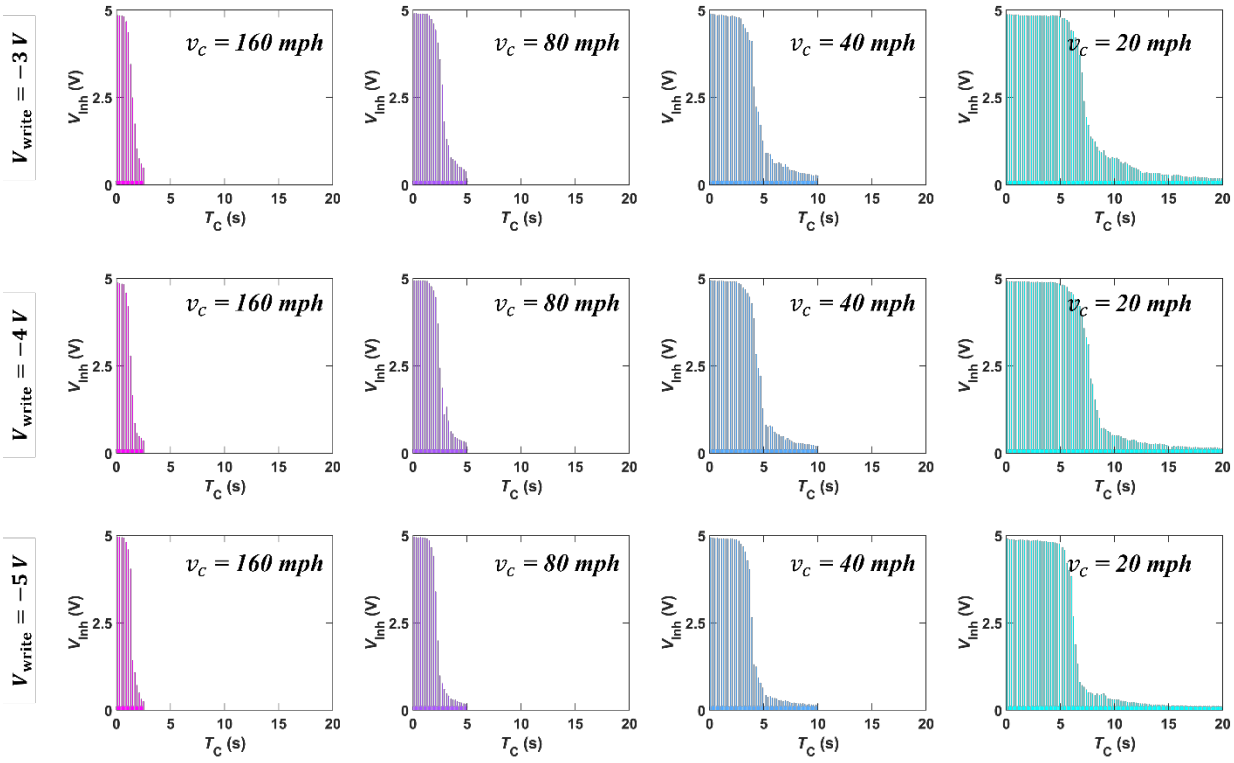

Figure S2. *Response of the inhibitory circuit to looming stimulus presented at various* V_{write}*, i.e., the temporal evolution of* V_{Inh} *measured at* V_{read} *= 0.5 V for various* v_c*.*

Supplementary Information 4.

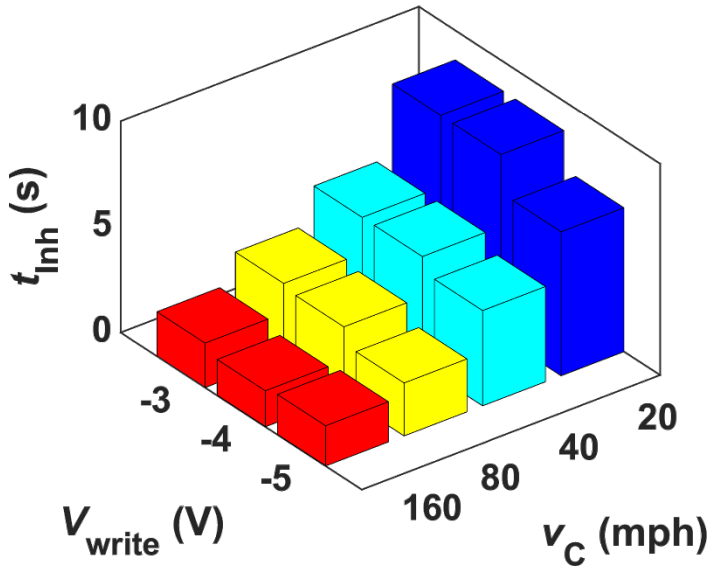

Figure S3. *Time to inhibition (t_{Inh}) plotted against different v_c and V_{write}.*

Supplementary Information 5.

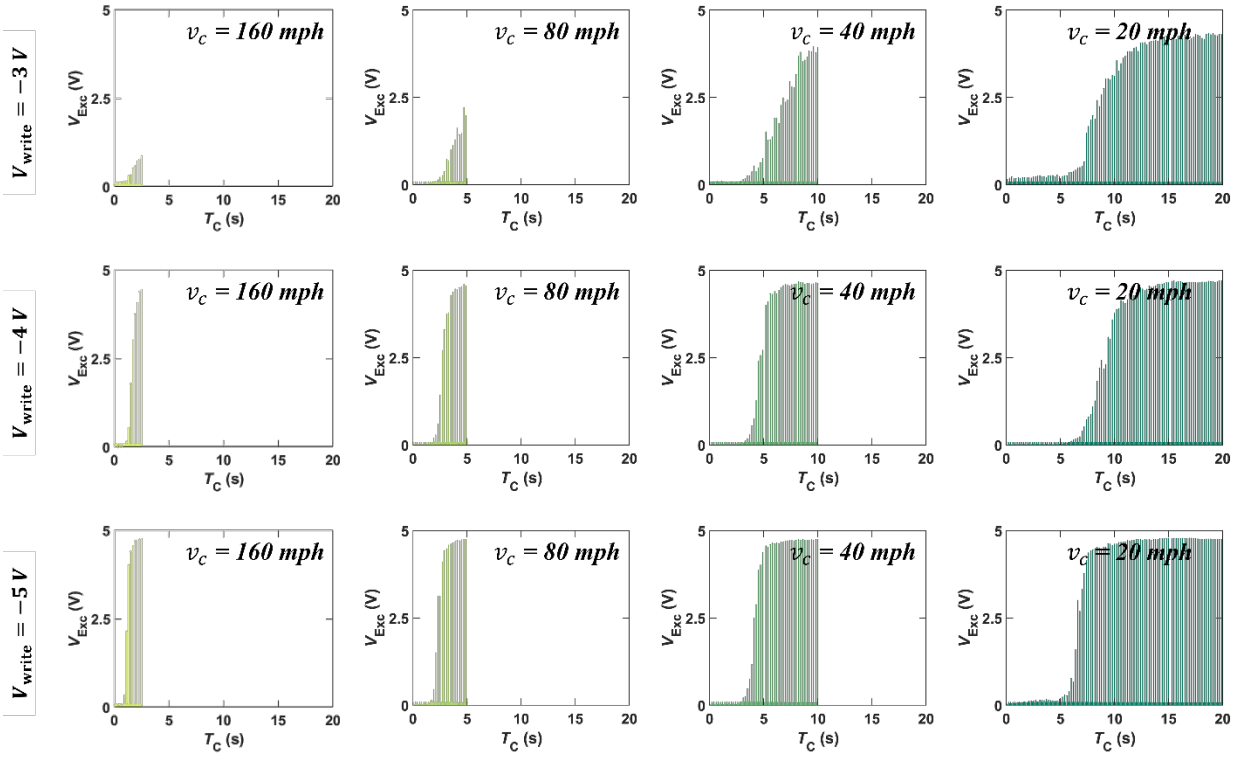

Figure S4. *Response of the excitatory circuit to looming stimulus presented at various* V_{write}*, i.e., the temporal evolution of* V_{Exc} *measured at* V_{read} *= 0.5 V for various* v_c*.*

Supplementary Information 6.

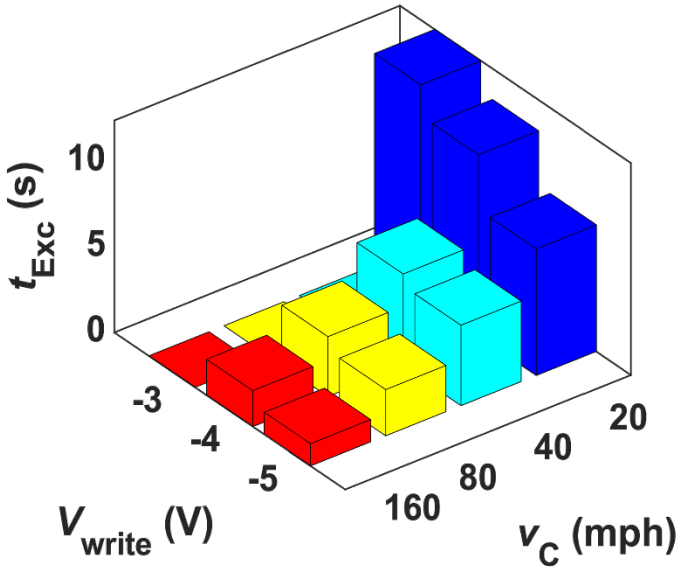

Figure S5. *Time to excitation (t_{Exc}) plotted against different v_c and V_{write}.*

Supplementary Information 7.

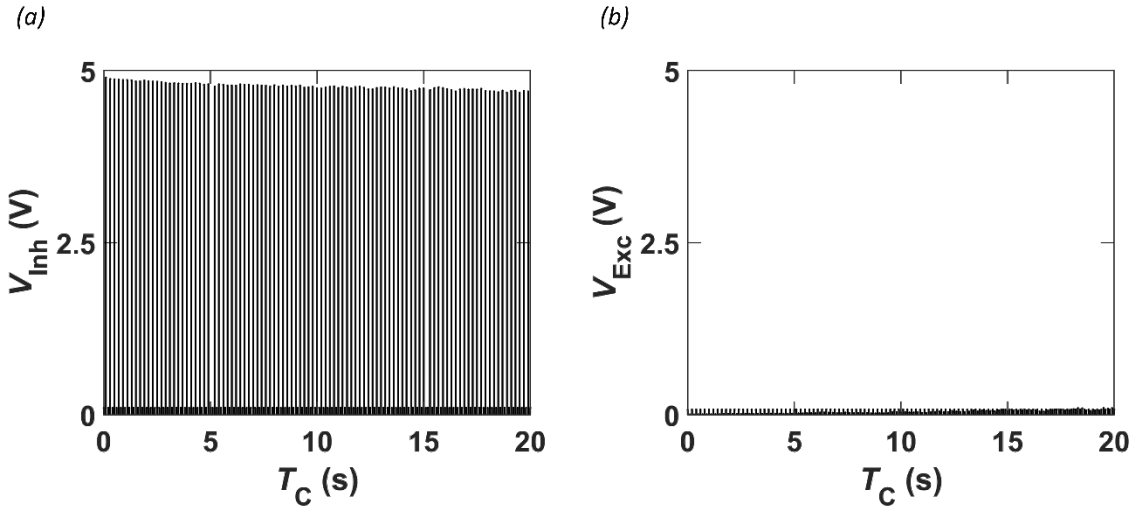

Figure S6. a) *Inhibitory and* ***b)*** *excitatory circuits show no transition, or, in other words, do not exhibit inhibition and excitation responses when measured in the absence of a looming stimuli.*

Supplementary Information 8.

I. Empirical Model of Excitatory and Inhibitory Circuit Outputs

Experimental results thus far have indicated the ability of the collision detector to generate spikes in response to impending collisions under varied looming rates and exposure conditions. In this section, we have described all empirical methods used to model outputs from individual modules and finally the escape response of the collision detector. Eq. S2, shown below, was used to model the output voltage of the inhibitory circuit.

$$V_{\mathrm{Inh}} = \frac{V_{\mathrm{DD}}}{1+e^{-\alpha(V_{\mathrm{IN}}-V_{SW})}} \qquad [S2]$$

Here, V_{Inh} is a function of the input voltage, $V_{\mathrm{IN}} = V_{\mathrm{N3}}$, threshold switching position, V_{SW}, drain voltage, V_{DD}, and a fitting parameter, α, that accounts for the slope of the circuit output while it is switching from V_{DD} to 0 V. The excitatory circuit was also modeled using the same function. Fig. S7a,b visually demonstrates the goodness of fit for these circuit characteristics while Table. S1 tabulates the parameters used for each circuit.

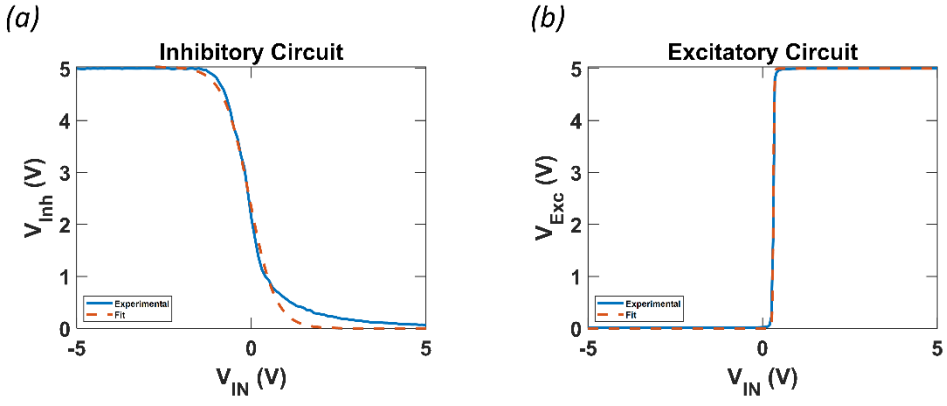

Figure S7. a) *Inhibitory and* ***b)*** *excitatory circuit characteristics and the corresponding fit using Eq. S2.*

	V_{DD} (V)	V_{SW} (V)	α
Inhibitory Circuit	5.0	-0.05621	-2.691
Excitatory Circuit	5.0	0.3091	72.16

Table S1. *Parameters used to fit excitatory and inhibitory circuit characteristics.*

II. Relation Between Switching Threshold of Inhibitory Circuit and Threshold Voltage of MT2

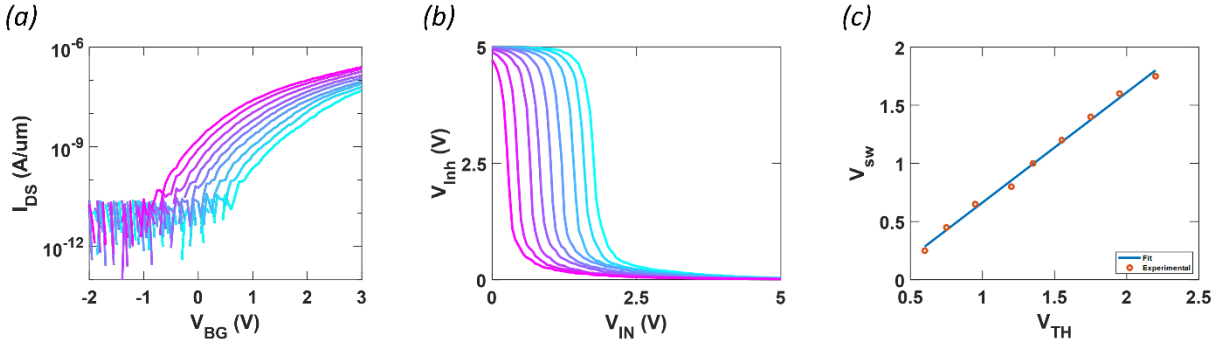

Figure S8. a) *Nine separate analog conductance states of MT2 corresponding to* ***b)*** *inhibitory circuit characteristics.* ***c)*** *Fit of the switching threshold of the inhibitory circuit (V_{sw}) as a function of the threshold voltage of MT2 (V_{TH}).*

An empirical model was used to relate the switching threshold of the inhibitory circuit, V_{sw}, to the threshold voltage of MT2, V_{th}. As shown in Fig. S8a above, MT2 was initially set at a low conductance state before being programmed eight times to create a total of nine differing conductance states. The constant current method was then used to extract the threshold voltage at each conductance state. Additionally, the output characteristics of the inhibitory circuit were measured at each conductance state of MT2 and are shown in Fig. S8b. The switching threshold of the inhibitory circuit was extracted as the point, V_{IN}, where $V_{Inh} = \frac{V_{DD}}{2}$. Fig. S8c shows V_{sw} of the inhibitory circuit as a function of V_{th} of MT2. A linear function, Eq. S3, was used to model

this relationship. The difference in α_1 and α_2 values between the inhibitory and excitatory V_{sw} will be negligible.

$$V_{sw} = \alpha_1 V_{th} + \alpha_2 \quad \text{[S3]}$$

III. Empirical Model of Photogating Behavior of MT2

An empirical model was used to simulate the photogating behavior of MT2. The shift in threshold voltage, ΔV_{TH}, as a function of the incident power seen at MT2, P_{IN}, the write voltage applied to *MT*2, V_{write}, and the time interval where the LED is turned on, t_{LED}, were experimentally extracted and modeled using Eq. S4 given below.

$$\Delta V_{TH} = -\gamma * P_{\mathrm{IN}}^{\beta} * \tau_{Exp} * \frac{V_{TH,max} - V_{TH}}{V_{TH,max} - V_{TH,init}} \quad \text{[S4]}$$

Here, γ and β are fitting parameters that determine the magnitude of the shift in threshold voltage of MT2 in response to an incident illumination for a given V_{write}. These parameters follow a linear relationship with V_{write} and can be expressed using Eq. S5a,b given below. Here, δ and ε are fitting parameters. $V_{TH,max}$ and $V_{TH,init}$ represent the maximum threshold voltage and the initial threshold voltage of MT2 before any light has been introduced, respectively. Furthermore, V_{TH} represents the threshold voltage of MT2 that varies at each time step, every time the device is exposed to new P_{IN}.

$$\gamma = \delta_1 * V_{write} + \delta_2 \quad \text{[S5a]}$$

$$\beta = \varepsilon_1 * V_{write} + \varepsilon_2 \quad \text{[S5b]}$$

Several P_{in} and V_{write} scenarios for fixed τ_{Exp} were evaluated experimentally and used to fit the γ and β parameters. Fig. S9a demonstrates the goodness of fit of Eq. S4 at three differing V_{write} levels. Fig. S9b,c visually demonstrates the linear dependence of γ and β on V_{write} and the goodness of fit for these parameters respectively.

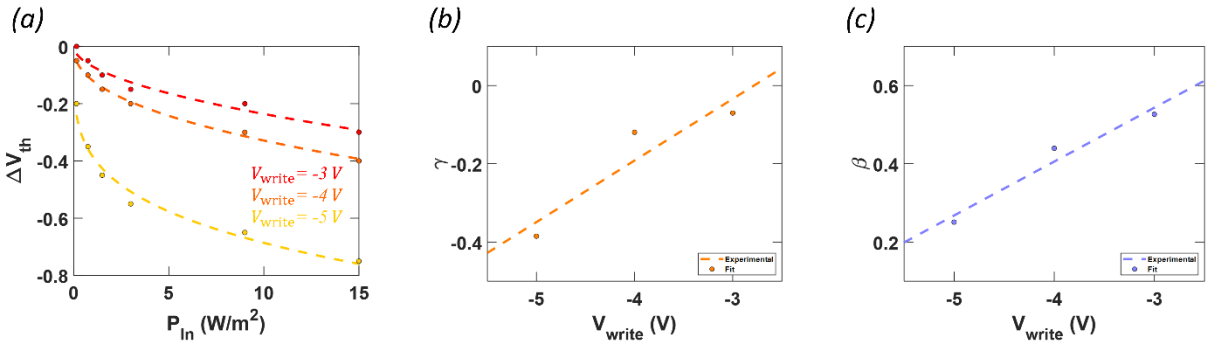

Figure S9. a) *Change in the threshold voltage, ΔV_{TH}, of MT2 as a function of incident power at three separate V_{write} magnitudes.* ***b)*** *Fit of γ as a function of V_{write} using Eq. S5a.* ***c)*** *Fit of β as a function of V_{write} using Eq. S5b*

IV. Empirical Model of Incident Illumination Intensity

The incident power of the front headlights of a 2021 Honda Accord were sampled at several distances between 58 ft and 454 ft. The incident power of the headlights was modeled as a function of distance using Eq. S6.

$$P_{\mathrm{IN}} = a * e^{b*d_c} \qquad [S6]$$

Here, a and b are fitting parameters. Fig. S1 visually demonstrates the goodness of fit of Eq. S6.

V. Empirical Model for Comprehensive Evaluation of Collision Detector

Thus far, empirical methods have been used to model the output characteristics of the inhibitory and excitatory circuits using Eq. S2 and the photogating behaviors of these circuits using Eq. S3 through S5. Field experiments of incident headlight illumination intensity have been modeled using Eq. S6. A compact model has been constructed that combines each of these individual equations and yields the spike output of the collision detector. For a given collision scenario, initially, the impending car will be at an initial position, d_c, from the ego vehicle, moving with a relative velocity, v_c. Eq. S6 is used to determine the incident power that would be seen at the collision detector. This changing incident power when presented to the collision detector over a time period of τ_{Exp} dictates a threshold shift in the inhibitory or excitatory circuits following Eq. S7.

$$\Delta V_{sw} = -\alpha_1 * (\delta_1 * V_{write} + \delta_2) * P_{\mathrm{IN}}^{\varepsilon_1 * V_{write} + \varepsilon_2} * \tau_{Exp} * \frac{V_{TH,max} - V_{TH}}{V_{TH,max} - V_{TH,init}} \quad [S7]$$

Next, the output voltage of the inhibitory and excitatory circuits is determined using Eq. S2. The inhibitory and excitatory circuits feed their output voltages into the gates of MT3 and MT4, respectively. The total charge in the channel of these transistors was simulated using Eq. S8a,b given below.

$$Q_{MT3} = Q_0 e^{\frac{q(V_{Inh} - V_{knee,MT3})}{m * K_B * T}} \quad [S8a]$$

$$Q_{MT4} = Q_0 e^{\frac{q(V_{Exc} - V_{knee,MT4})}{m * K_B * T}} \quad [S8b]$$

Here, m, K_B, T, and q represent the body factor of MT3, the Boltzmann constant, temperature, and the elementary charge of an electron, respectively. V_{knee} represents the knee point of MT3, i.e.,

the input voltage corresponding to the I_{DS} = 10 pA. Q_0 is a constant. The charge values in the channels of MT3 and MT4 are then converted into conductance values which can be summed as resistors in series. Finally, the output current of the collision detector is calculated using Ohm's Law.

References

[1] F. Gabbiani, H. G. Krapp, C. Koch, and G. Laurent, "Multiplicative computation in a visual neuron sensitive to looming," *Nature,* vol. 420, no. 6913, pp. 320-324, 2002/11/01 2002, doi: 10.1038/nature01190.

[2] F. Gabbiani, H. G. Krapp, and G. Laurent, "Computation of Object Approach by a Wide-Field, Motion-Sensitive Neuron," *The Journal of Neuroscience,* vol. 19, no. 3, pp. 1122-1141, 1999, doi: 10.1523/jneurosci.19-03-01122.1999.